
Supplementary Material for
Large negative Poisson's ratios and multiple single-spin Dirac cones in 2D VOX (X =
F, Cl, Br, I) monolayers

Shuzhen Li¹, Huabin Gong¹, Yanju Ji¹, Han Gao¹, Ying Chen¹, Bo Yang^{*1}, Mingwen
Zhao^{*2}

1 School of Science, Shandong Jianzhu University, Jinan, 250101, Shandong, China

2 School of Physics, Shandong University, Jinan, 250100, Shandong, China

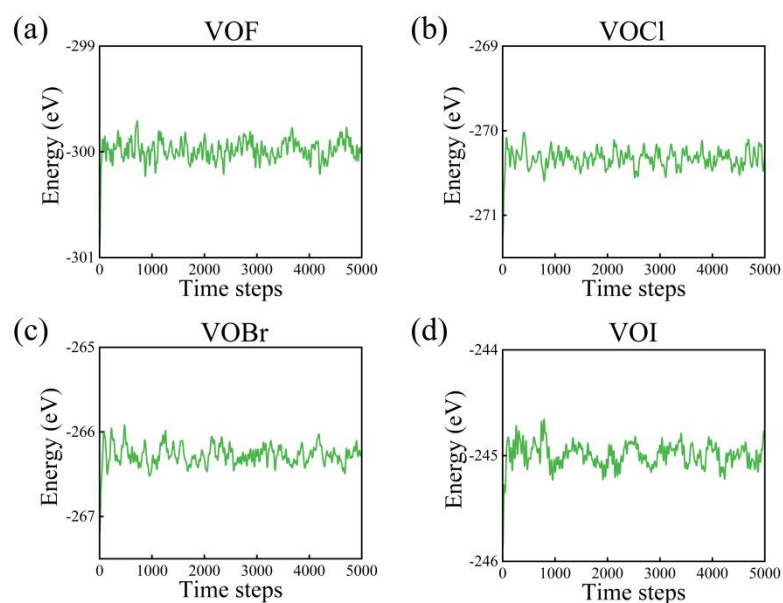


Fig. S1. The temporal evolution of total free energy during AIMD simulations at 300 K of (a) VOF, (b) VOCl, (c) VOBr and (d) VOI.

	$a(\text{\AA})$	$b(\text{\AA})$	V-O(\AA)	V-X(\AA)	$h(\text{\AA})$
VOF	3.328	3.399	1.787	1.951	1.613
VOCl	3.265	3.112	1.799	2.284	2.429
VOBr	3.309	3.320	1.808	2.421	2.493
VOI	3.419	3.660	1.824	2.597	2.482

Table S1. Structural parameters of the VOX (X = F, Cl, Br, I). The lattice constants a

and b , thickness h of VOX.

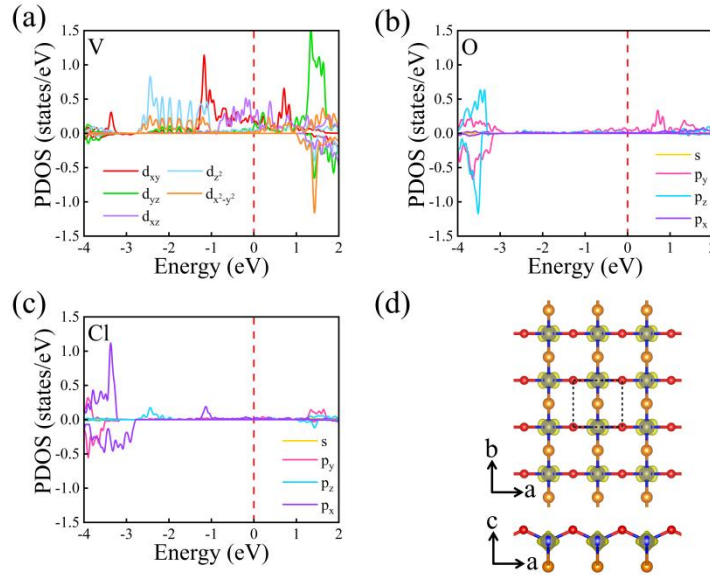


Fig. S2. We also calculated the projected density of states (PDOS) for VOCl, as shown in Fig. S1(a)-(c). The results reveal that the electronic states near the Fermi level are predominantly contributed by the d -orbitals of V atoms, particularly the d_{xy} , d_{yz} , d_{xz} orbitals, which exhibit significant density within the energy range of -2 eV to 2 eV. This confirms that the half-metallic properties and magnetic behavior of VOCl are primarily driven by the d -orbital electrons of V atoms, while the contributions of the O and Cl atoms, as well as the s , p_x , p_y , p_z orbitals of V atoms, are negligible near the Fermi level, which is consistent with the Kohn-Sham wave functions, as shown in S1(d).

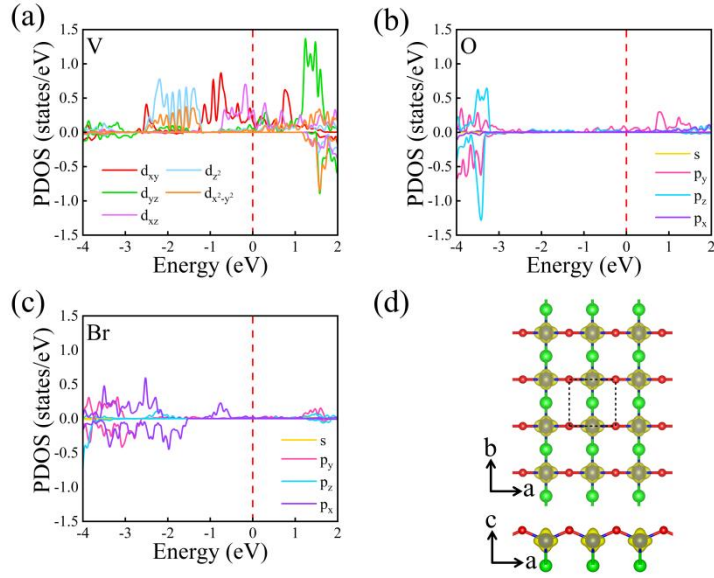


Fig. S3. We also calculated the projected density of states (PDOS) for VOBBr, as shown in Fig. S2(a)-(c). The results reveal that the electronic states near the Fermi level are predominantly contributed by the d -orbitals of V atoms, particularly the d_{xy} , d_{yz} , d_{xz} orbitals, which exhibit significant density within the energy range of -2 eV to 2 eV. This confirms that the half-metallic properties and magnetic behavior of VOBBr are primarily driven by the d -orbital electrons of V atoms. While the contributions of the O and Br atoms, as well as the s , p_x , p_y , p_z orbitals of V atoms, are negligible near the Fermi level, which is consistent with the Kohn-Sham wave functions, as shown in S2(d).

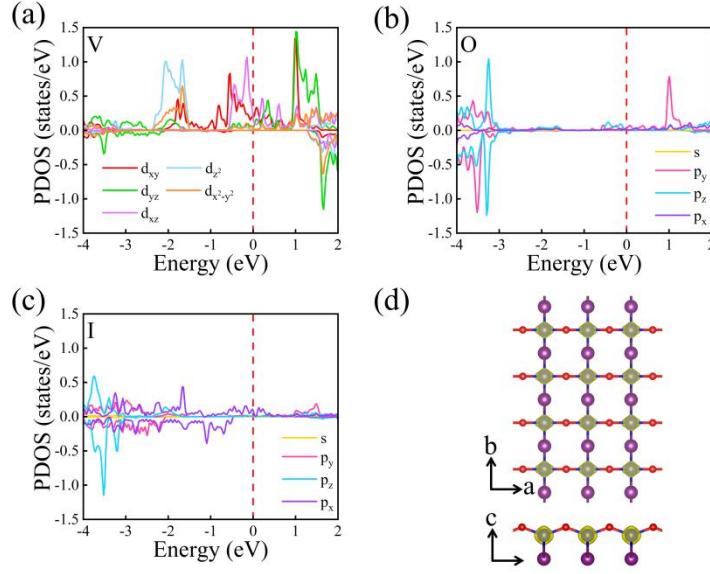


Fig. S4. We also calculated the projected density of states (PDOS) for VOI, as shown in Fig. S3(a)-(c). The results reveal that the electronic states near the Fermi level are predominantly contributed by the d -orbitals of V atoms, particularly the d_{xy} , d_{yz} , d_{xz} orbitals, which exhibit significant density within the energy range of -2 eV to 2 eV. This confirms that the half-metallic properties and magnetic behavior of VOI are primarily driven by the d -orbital electrons of V atoms. While the contributions of the O and I atoms, as well as the s , p_x , p_y , p_z orbitals of V atoms, are negligible near the Fermi level, which is consistent with the Kohn-Sham wave functions, as shown in S3(d).

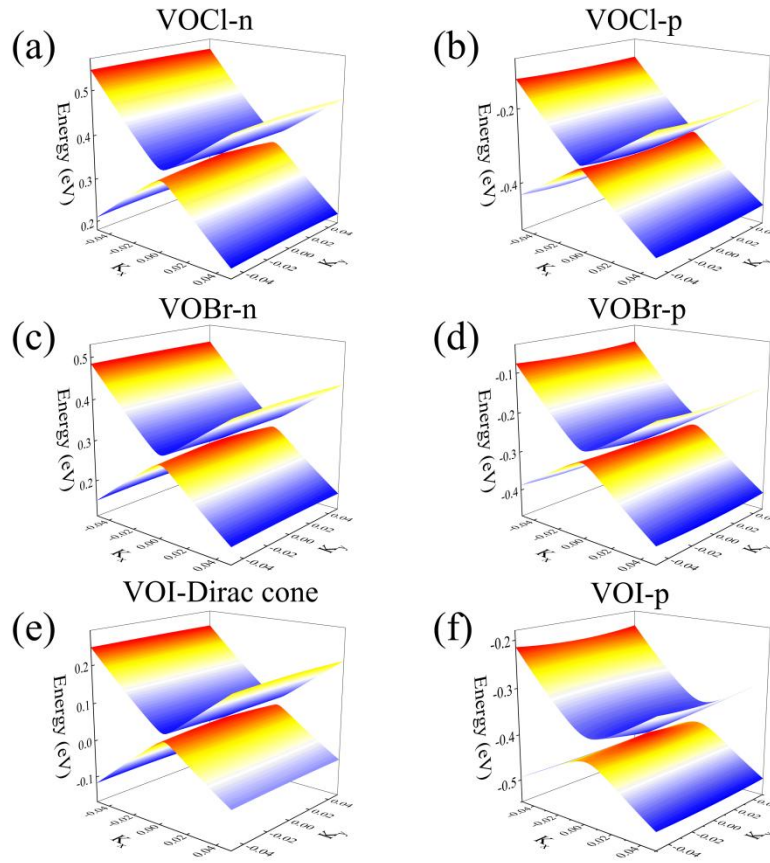


Fig. S5. (a) Three-dimensional band structure of n-type single-spin Dirac point and (b) p-type single-spin Dirac point near the Fermi surface in monolayer VOCl. (c) Three-dimensional band structure of n-type single-spin Dirac point and (d) p-type single-spin Dirac point near the Fermi surface in monolayer VOBr. (e) Three-dimensional band structure of n-type single-spin Dirac point and (f) p-type single-spin Dirac point near the Fermi surface in monolayer VOI. The Fermi level is set to 0 eV.

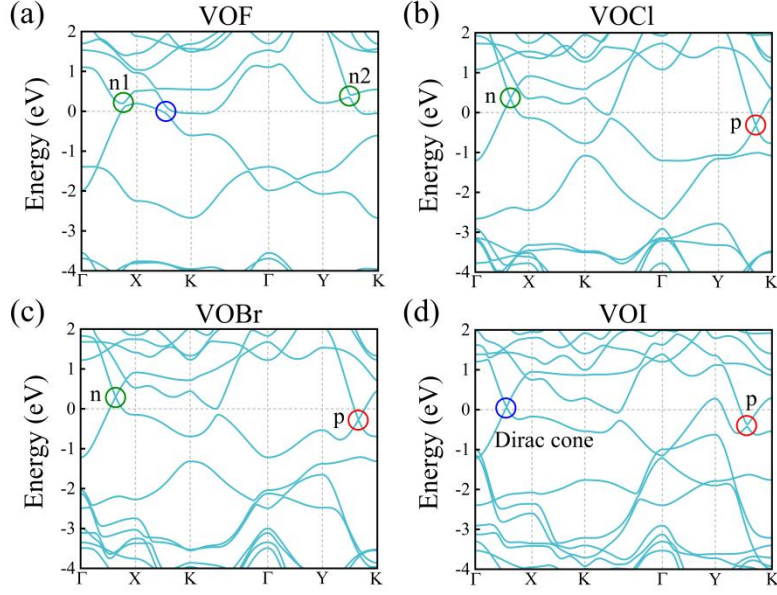


Fig. S6. The electronic band structures with spin-orbit coupling (SOC) of (a) VOF, (b) VOCl, (c) VOBr and (d) VOI monolayer.

structures	carrier types	Band gap (meV)
VOF	n1	76
	Dirac cone	164
	n2	67
VOCl	n	32
	p	28
VOBr	n	18
	p	26
VOI	Dirac cone	12
	p	53

Table S2. The gap of single-spin Dirac cones/Dirac points of VOX (X = F, Cl, Br, I) with spin-orbit coupling (SOC).

	$E_f(\text{monolayer})/\text{eV}$	$E_f(\text{bulk})/\text{eV}$	V-O/Å	V-X/Å
VOF	-1.983	-2.351	1.886(2.074)	2.013
VOCl	-1.496	-1.747	1.881(2.131)	2.385
VOBr	-1.324	-1.556	1.888(2.134)	2.540
VOI	-1.077			

Table S3. $E_V, E_O, E_F, E_{Cl}, E_{Br}$ and E_I were calculated by Vanadium bulk, O₂, F₂, Cl₂, Br₂ and I₂ molecule, respectively. The energy of V, O, F, Cl, Br and I atom was $E_V =$

-9.94eV, $E_O = -4.84\text{eV}$, $E_F = -1.86\text{eV}$, $E_{Cl} = -1.79\text{eV}$, $E_{Br} = -1.49\text{eV}$, $E_I = -1.31\text{eV}$. The formation energy of VOX was defined as follows: $E_f = (E_{VOX} - E_V - E_O - E_X)/3$, where E_{VOX} represents the total energy of the VOX ($X = \text{F, Cl, Br, I}$). The calculated results are presented in Table S1. The negative formation energies indicate that the monolayers are energetically favorable. Furthermore, the bulk structures of VOF, VOCl and VOBr, with the $Pmmn$ space group, were also subjected to energy calculations, with the formation energy formula modified to $E_f = (E_{V_2O_2X_2} - 2E_V - 2E_O - 2E_X)/6$; the computational results are presented in Table S1. A comparative analysis of formation energies between VOX ($X = \text{F, Cl, Br}$) bulk and monolayer phases reveals that the bulk phase exhibits a lower formation energy of approximately 0.3 eV/atom. However, the study reveals that both V-O and V-X bond lengths in VOX ($X = \text{F, Cl, Br}$) monolayers are significantly shorter than their counterparts in bulk materials. This bond contraction indicates stronger chemical bonding in the monolayer structure, shown in Table 1, elucidating stronger chemical bonding within the 2D configuration, concomitantly suggesting enhanced chemical stability despite the higher formation energy.

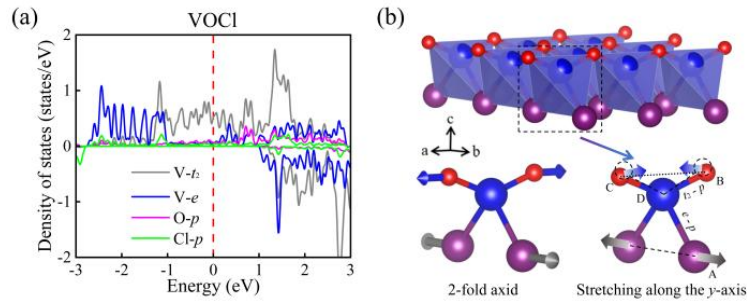


Fig. S7. (a) Atom-projected density of states (DOS) of VOCl. The DOS shown in the figure are t_2 (d_{xy} , d_{yz} , d_{zx}), e ($d_{x^2-y^2}$, d_z^2) and p (p_x , p_y , p_z). The Fermi level is set to zero. (b) The Poisson's ratio in monolayer VOX ($X = \text{F, Cl, Br, I}$) arises from the coordination of each V atom with two O atoms and two X atoms, forming a slightly distorted VO_2X_2 tetrahedron. The schematic of stress application (gray arrows) in the lower left, perpendicular to the two-fold axis, and the resulting motion (blue arrows) exhibits a negative Poisson's ratio. The stress schematic in the lower right illustrates

the motion of O atoms (blue arrows) within the B–D–C plane under tensile strain along the y -axis (gray arrows) in the VOCl, demonstrating a positive Poisson's ratio.

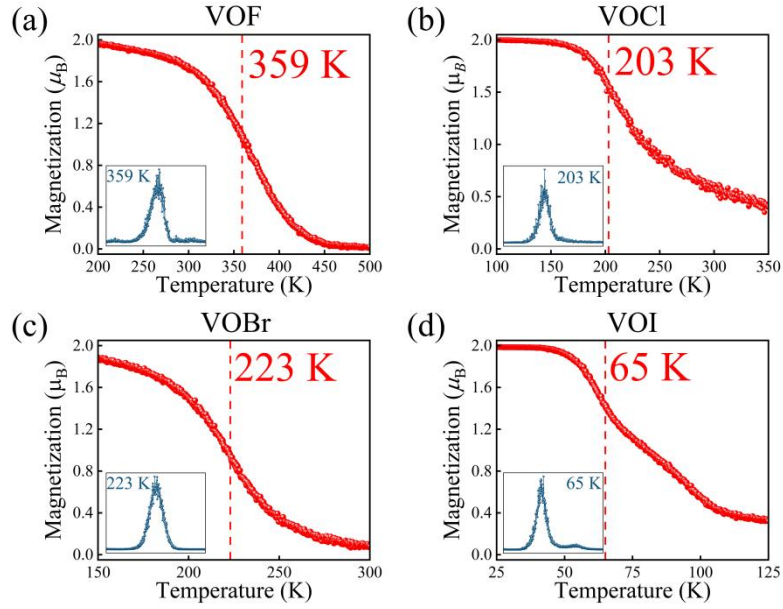


Fig. S8. Monte Carlo simulations based on the Ising model illustrate the temperature dependence of the magnetic moments for (a) VOF, (b) VOCl, (c) VOBr and (d) VOI. The accompanying figures depict the variation of the specific heat capacity (C) of VOX ($X = F, Cl, Br, I$) across different temperatures, with all physical quantities normalized.
